Manipulation of Streamwise Vorticity in an Emulated Diffuser Boundary Layer Using Hybrid Flow Control

Abraham N Gissen*, Bojan Vukasinovic†, and Ari Glezer‡
Woodruff School of Mechanical Engineering,
Georgia Institute of Technology, Atlanta, GA 30332-0405

The formation and interaction of streamwise vorticity generated by surface-mounted passive (micro-vanes) and active (synthetic jets) flow control elements is investigated experimentally in a small-scale wind tunnel at high subsonic speeds ($M < 0.6$). Streamwise vortices are generated within the boundary layer of a converging-diverging wall insert that is designed to provide an adverse pressure gradient similar to the pressure gradient within a typical offset diffuser. Hybrid actuation is demonstrated by combining the micro-vanes with synthetic jets in tandem or by integrating the jets into vanes. Tandem actuation is accomplished using synthetic jet actuators that are yawed to match the vanes' yaw angle and skewed to generate streamwise vortices of matching sense. Both approaches lead to augmentation of the primary vanes' vortices and enhance their pairing. These approaches provide "fail-safe" control devices having robust nominal control effectiveness by the vane elements coupled with enhancement by the jets.

I. Introduction

I.1 Technical Background

Development of embedded propulsion systems for high efficiency aircraft, such as the blended wing body (Liebeck 2004), dictates the inclusion of complex inlet geometries. The interaction between the evolution of secondary flows, complex entrance flows, and separation within such ducts results in low recovery and flow distortion at the engine face over large parts of the flight envelope with significant consequences for efficiency (Bansod and Bradshow 1972). Ingestion of the boundary layer formed over the aircraft's wing further degrades the performance of the inlet (Berrier and Allan 2004, Berrier et al. 2005). However boundary layer ingestion has been shown to decrease overall necessary propulsive power (Smith 1993, Plas et al. 2007) and thereby fuel burn rates by an estimated 10% when compared with external nacelles (Kawai et al. 2006). The addition of flow control to the inlet of the proposed blended wing body design has the potential for even further systems-level improvements in performance by enabling weight and wetted area reductions (Daggett et al. 2003). Passive flow control in an s-duct was demonstrated by Anderson and Gibb (1993) whereby a row of vane type vortex generators in an s-duct induced properly structured near wall vorticity to reduce distortion and increase pressure recovery at the exit plane of the inlet. Owens et al. (2008) installed a similar single row of vortex generators into an s-duct operating in a free stream at $M = 0.85$, using a model that more closely resembles the blended wing body flush-mounted s-duct. Boundary layer ingestion and the control of the resulting flow field using similar passive flow control devices was studied by Anabtawi et al. (1999) and Tournier and Paduano (2005). The induced drag associated with vanes was

* Graduate Research Assistant, AIAA Member.
† Research Engineer, AIAA Member.
‡ Professor, AIAA Associate Fellow.

decreased through the use of sub-boundary layer devices (Anderson et al. 2002). These micro-vanes demonstrated effective AIP (aerodynamic interface plane) distortion management in more aggressive compact s-ducts (Anderson et al. 2004a) using small scale vanes showing successful applications in compact s-ducts. Experimental work by Jirásek (2006) on complex, D-throat, heavily serpentined inlets further corroborated the flow control authority of sub-boundary layer vane installations. Despite the advantages inherent to these robust and reliable passive devices, they cannot respond to temporally varying structures produced while navigating through a broad flight envelope. Consequently, vanes are generally sized for the extremes of the flight envelope which can result in excess drag under more optimal conditions.

With the advantages of having instantaneous control and little or no drag penalty when not energized, active flow control is a very attractive option for the control of flow in an s-duct. Anderson et al (2004b) preformed a design of experiments to optimize the installation of jets emanating from the inner surface of an inlet duct, which increased pressure recovery and decreased engine face distortion. Vortex generating jets installed in a more complex serpentine inlet duct showed drastic improvements in distortion levels and slight improvements in drag in a study performed by Scribben et al. (2006). Optimization of the placement of similar discrete jets by Owens et al. (2008) in a flush mounted serpentine inlet with an imposed free stream of M = 0.85 indicated efficacy of such jets in a flow field similar to that which could be used on the blended wing body. A variety of locations and configurations of different flow injection were tested with resulting insight into the most effective and most efficient implementation for these particular jets. Vaccaro et al. (2010) showed that the use of Coanda surfaces along with various spanwise continuous jet configurations was effective at controlling the pressure recovery and reducing the intensity of the structures produced by the separation found in a rectangular offset duct. The parasitic use of bleed air was demonstrated to be avoidable for active flow control in ducts at low speeds by Amitay et al. (2008) who successfully used synthetic jets, which require zero mass flux, to control flow separation in an offset duct. While active actuation approaches can be adapted to provide feedback control in flight, the system can be complex and often requires significant engine bleed. In addition, the inlet still needs to be designed to perform over a broad range to ensure active flow control fail-safe operation (Kawai et al. 2006).

Figure 1. *Surface oil-flow visualization of the streamwise vortices generated by passive micro-vane control elements in an offset diffuser.*

A hybrid approach, demonstrated by Owens et al. (2008), which combined both active and passive flow control improved performance across the entire controlled regime especially at inlet mass flow rates where the passive flow control devices were not optimized. Anderson et al. (2009), in an effort to reduce the quantity of engine bleed required, used active flow control to enhance the vorticity produced by the passive flow control devices. The study combined the micro-ramps used in Anderson et al. (2006) with flow injection resulting in an almost ten-fold reduction in required engine bleed.

I.2 Controlled Streamwise Vortices in Diffuser Configurations

Typical passive control of the secondary flow in an offset diffuser consists of an array of flow control vanes which generate the corresponding array of single-sign vortices over each side of the diffuser span. An example of such control is shown in Figure 1 as a surface oil-flow visualization of the flow on one side of an offset diffuser. This array of single-sense vortices merge as they evolve in the downstream direction, and oppose the flow rotation by the secondary flow. It is a main objective of the present work to examine approaches of integration of active control elements along with such passive vanes to augment the 'baseline' vane effect in an active manner. Furthermore, the active control elements consisting of synthetic jet actuators were chosen due to their inherent advantage of zero net mass flux that does not require external air supply.

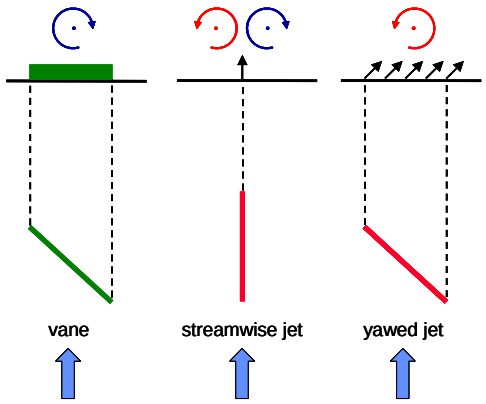

Figure 2. *Schematics of a single-sign and counterclockwise pair of streamwise vortices generated by a micro-vane and synthetic jet.*

Gissen et al. (2009) presented fluidic counterparts of passive inlet control elements where unsteady single and counter rotating streamwise vortices were actively formed by streamwise-oriented and yawed synthetic jet configurations, respectively. A summary of their findings relevant for integration of active control elements with micro-vane configurations is shown in Figure 2. A single-sense vortex produced by a micro-vane (Figure 2*a*) induces an upwash on the trailing side of the vane. To mimic such generation of a single-sense streamwise vorticity by a synthetic jet, it was shown that a nominally streamwise-oriented jet orifice (Figure 2*b*) can be yawed with respect to the free stream (Figure 2*c*). However, it was also shown (Gissen et al. 2009) that the single streamwise vortex that is formed by a yawed synthetic jet has the opposite sense than the vortex generated by a micro-vane having the same yaw orientation (as schematically shown in Figures 2*a* and *c*). Hence, a direct pairing of passive vanes and active yawed jets would impose detrimental limitations on spanwise spacing of the control elements, as active yawed jets would need to be yawed in the opposite direction to the vanes in order to generate same-sense vorticity.

The synthetic jet actuators are used to augment the passive elements in hybrid configurations with a broader, controllable operating range having an inherent fail-safe margin. The use of synthetic (zero net mass flux) jet actuators obviates the need for supply of bleed air and therefore of complex fluidic plumbing and integration. A schematic diagram of a synthetic jet in a 'tandem' configuration with a micro-vane is illustrated in Figure 3. In this approach, the synthetic jet orifice is yawed to conform to the vane orientation, and is also skewed relative to the surface to determine the sense of the ensuing vortex. This combination of active and passive elements creates a fail-safe adjustable hybrid flow control device that can lead to highly-

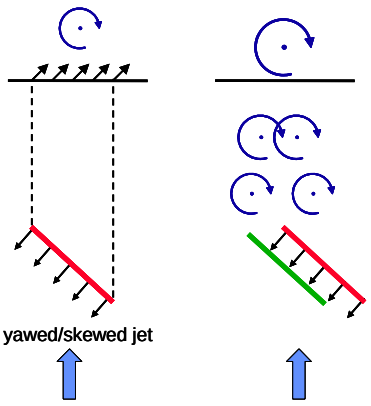

Figure 3. *Schematics of a single-sign vortex generated by the yawed/skewed synthetic jet and of its 'tandem' integration with a passive vane.*

effective performance enhancements of embedded propulsion systems with minimal system-level penalties in terms of weight, power consumption, robustness and maintenance.

III. Experimental Setup and Procedures

The experiments are performed in an open-return, pull-down high-speed subsonic wind tunnel (test sections speeds of up to $M = 0.75$) which is driven by a 150 HP blower. The modular test section (Figure 4) measures 12.7 × 12.7 × 61 cm, and the temperature of the return air is controlled using a chiller coupled with an ultra low pressure drop heat exchanger. The upper wall of the test section is fitted with a converging-diverging insert to impose an adverse pressure gradient of $\mathrm{d}p/\mathrm{d}x \approx 0.38 \cdot p_s/L$ which closely matches the pressure gradient in a typical offset diffuser.

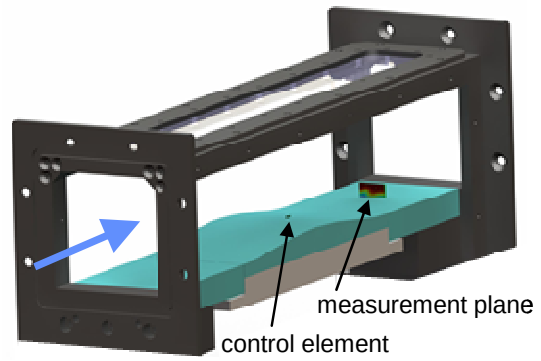

Figure 4. *Test section with a profiled wall. Locations of the control elements and the measurement plane are marked at the wall.*

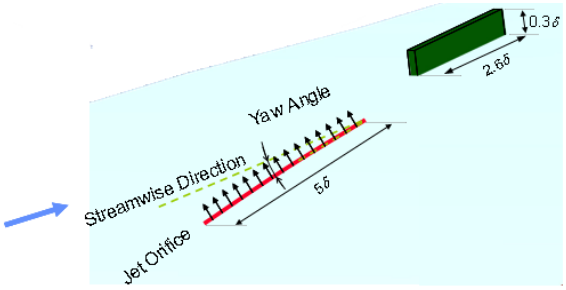

Figure 5. *Schematics of micro-vane and synthetic jet module with respect to flow. Both control elements are yawed relative to the streamwise direction, and the jet is issued at a skew angle relative to the surface.*

Various configurations of passive (micro-vane) and active (synthetic jet) flow control actuators are surface mounted immediately downstream of the apex of the converging-diverging test section insert. The downstream position for the PIV characterization of the flow is selected such that it corresponds to the AIP in the emulated offset diffuser, and is located at $x/\delta = 42$ ($\delta = 5$ mm at the apex with an upstream $M = 0.5$) downstream from the wall apex. All experiments were performed for an upstream $M = 0.5$.

Schematic descriptions of the individual control devices are shown in Figure 5. The micro-vane is 0.3δ high and 2.6δ long, and is yawed by 8°. The synthetic jet orifices measure 25 × 0.5 mm and can operate within the range 1-2.5 kHz. The skewed/yawed jet orifice is nominally aligned with the micro-vane, and issues a jet at 45° to the surface. The present synthetic jets are calibrated using simultaneous, phase-locked measurements of the jet exit velocity, piezoelectric disk (centerline) displacement and cavity pressure and temperature, as described in more detail by Gissen et al. (2009). Individual control elements

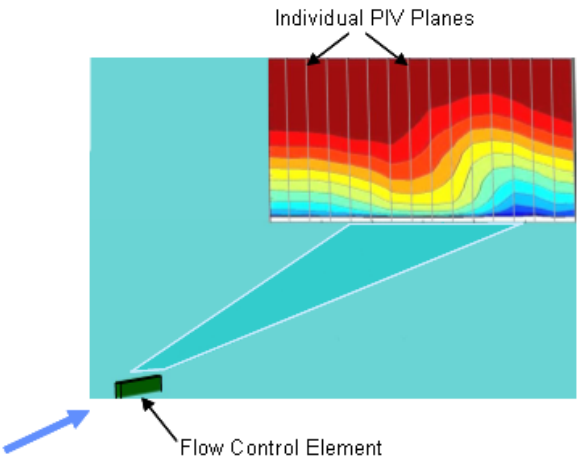

Figure 6. *Representation of PIV measuring station and measuring planes with respect to the flow control element.*

are combined in various tandem and integrated configurations that are further defined in the reminder of the paper.

Diagnostics include high-resolution, high-speed PIV measurements at multiple cross stream (x-y) planes of the flow fields that are spaced 2 mm apart across the span. The PIV field of view measures 15 mm on the side and the magnification is 17 μm/pixel. The outline of the PIV measurement station is shown in Figure 6 for a single micro-vane configuration, where each of the measured (x-y) planes is seen as a line. Such measured (x-y) flow fields are afterwards composed together into the (y-z), cross-sectional flow fields. The resulting (y-z) flow field of the mean streamwise velocity component U is shown in Figure 6. Further processing of the measured flow fields is performed to assist in the illumination of the flow structures, which is illustrated in Figure 7. The 'far-field' effect of the micro-vane on the boundary layer is elucidated from a color raster plot (with contours) of composite time-averaged streamwise velocity distribution $U(y,z;x)$ (Figure 7*a*). These distributions indicate a clear downwash effect at center span ($z/\delta_{apex} \approx 0$) which is accompanied by the upwash peak at about $z/\delta = -2$. These effects are a direct consequence of the induced streamwise vortex formed by the micro-vane. To better isolate the effect of the streamwise vortex, the streamwise velocity increment (decrement) relative to the baseline flow (in the absence of actuation, Figure 7*b*) $\Delta U(y,z;x)$ is typically derived from the initial composite flow field, and the resulting velocity difference is shown in Figure 7*c*. Owing to the presence of the wall, the cross stream elevations of the peaks (positive and negative) of ΔU (Figure 7*c*) are different. The deficit owing to the upward advection of low-momentum fluid is farther away from the surface than the high-momentum fluid and the transported high-momentum concentration appears to spread in the spanwise direction along the surface. All the composite flow fields in the remainder of the paper are shown as ΔU (or V) differences relative to the baseline flow field.

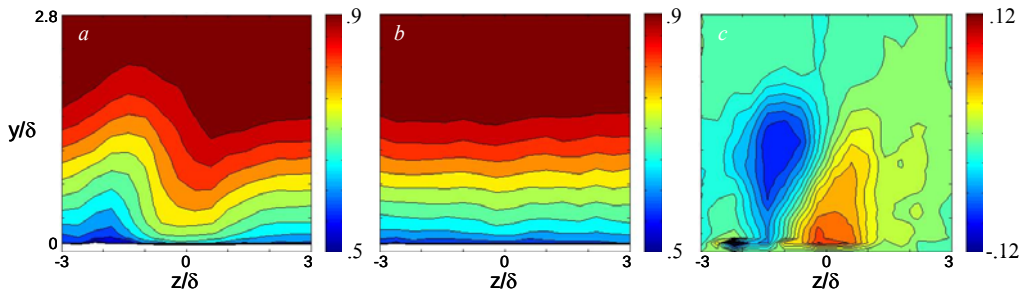

Figure 7. *Composite raster plot of the streamwise component of velocity U/U_0 for the nominal micro-vane control (a) and the baseline uncontrolled flow (b), and their velocity difference $\Delta U/U_0$ (c).*

IV. Results

IV.1 Synthetic Jet Orifice Orientation

As noted in Section I, active generation of single-sense vortices using synthetic jets can be done by either yawing (relative to the free stream) or skewing (relative to the exit plane) of the surface-embedded jet orifices. In order to conform to the passive vane orientation, it is preferable to have the jets orifices yawed along the same direction, but it was shown that such orientation generates streamwise vorticity of the opposite sense to the vanes (Gissen et al. 2009). To preserve the preferable jet orientation and generate the same sense of vorticity as the vanes, it is proposed that the orifice is also adequately skewed and issues under a nonorthogonal skew angle relative to the surface. Preliminary tests (not shown) of the skew angles between 30° and

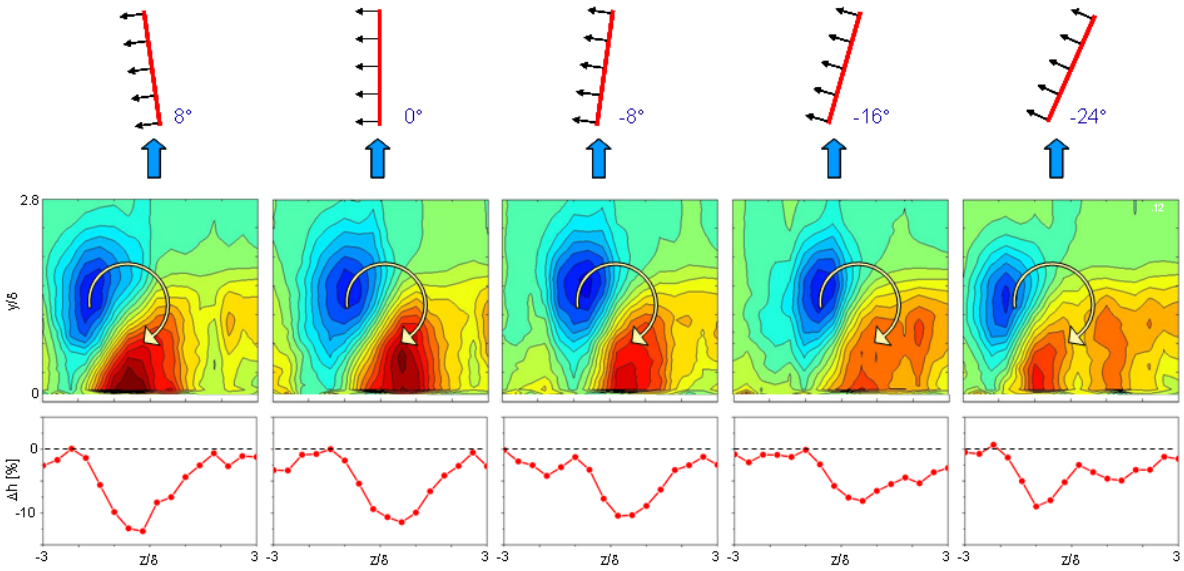

Figure 8. *Effect of the orifice yaw angle (top row) on the velocity deficit $\Delta U/U_0$ (middle) and the boundary layer shape factor Δh (bottom).*

60° degrees indicated weak dependence on the skew angle, and it was set at 45° for the reminder of the study.

Sensitivity of the strength of the single sense vorticity which results from this type of yawed and skewed jet was studied first by varying the yaw angle for a constant skew angle (Figure 8). When the synthetic jet orifice is aligned with the flow (Figure 8*b*), a single sign vortex is formed, which sense is governed by the direction of skew of the orifice. As the jet is yawed at nonzero angle, the spanwise projection of the orifice increases and induced vorticity gives rise to its spanwise component along with predominant streamwise component. Therefore, with an increase in the yaw angle (Figure 8*c*–*e*), a clear trend of increased spanwise domain of influence and decreased effect magnitude is measured. It is also seen that the yaw angle matching the vane orientation (Figure 8*a*) slightly increases the far-field area of influence and also somewhat reduces velocity deficit. A cross-stream integral effect of these active control configurations on the boundary layer flow is assessed from the relative spanwise changes in the shape factor *h*. The shape factor is calculated from the measured cross-stream velocity distributions in the absence and presence of the jets, and the corresponding spanwise profiles are shown as a percentage change relative to the baseline at the bottom row in Figure 8. First, it should be noted that overall effect of any of the configurations is favorable, as the shape factor is either decreased or virtually unchanged across the measured span. The effect typically spreads over $\Delta(z/\delta) = 4$, with a general trend of decreasing magnitude and extending span of influence with an increase in the yaw angle.

Based on this study, the jet orifice yawed at the same angle as the micro-vane is shown to generate the favorable far-field effect while preserving a convenience for any tandem integration of the jets and the vanes in a hybrid control device. Therefore, a synthetic jet having a yaw angle of 8° and the skew angle of 45° is selected for all the following integration studies.

IV.2 Hybrid Tandem Configurations

The first approach in combination of the pre-selected passive and active control elements is motivated by facilitation of a favorable merging and augmentation of individually-created single-sense streamwise vortices, much like in the case of an array of exclusively passive devices. This approach required a placement of vanes and jets at a certain spatial configuration, which was initially sought after by kinematic considerations of individual effects of the control elements. Based on the known locations of each of the tested elements, and its measured spanwise extent of the effect, an initial spacing between the micro-vane and synthetic jet was estimated. As an example, two configurations illustrating interacting and non-interacting vortices are shown in Figure 9. Figure 9*a* shows an example where two control elements are spaced close enough to promote merging of the individual vortices, while the two control elements are spaced apart enough to just begin to interact at the measurement plane in Figure 9*b*. Due to a typical short overall length of an inlet diffuser, it is clearly an advantage if the interaction length of individual control vortices is reduced, i.e., if individual vortices begin to interact right after their formation.

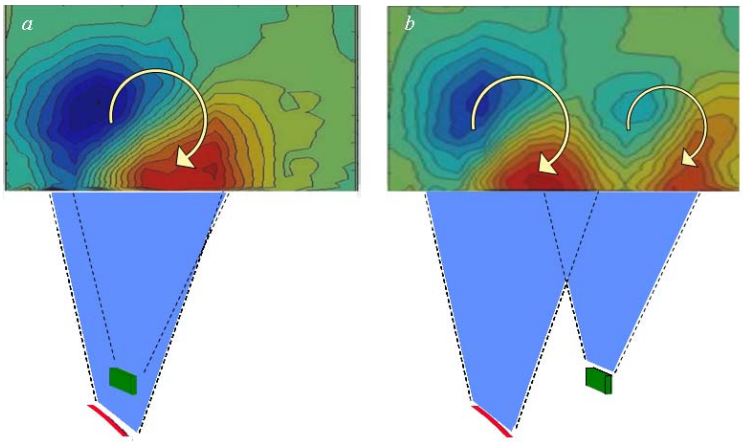

Figure 9. *Illustration of the spanwise spacing between the passive and active control elements that results in strong (a) and weak (b) vortex interaction.*

Once an initial estimate of the spacing between the vane and the jet was made, two additional variations of the spacing were selected such that the vane spacing was set on either side of the jet. These three spanwise distributions are combined with positioning of the vane either upstream or downstream from the jet (defined as v1 – v3 in Figure 10). The vane was placed both upstream and downstream in various locations to provide insight into the nonlinear superposition of the two distinct resulting flow fields. All six configurations are defined in Figure 10.

The results for the three spanwise spacings of the vane upstream from the jet are shown in Figure 11 in terms of the mean field difference ΔU, as defined in conjunction with Figure 7, in the absence and presence of the jet. As the vane is moved in the positive spanwise (z) direction, the resulting vortex formed off the vane consequently shifts within the measured field of view (Figure 11, Jet OFF). The vortex imprint spans approximately 3δ and it is fully captured in the measurement domain only in the v1 configuration. As the jet is activated in any of

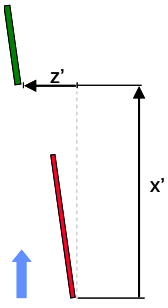

vane location	config	x'/δ	z'/δ
downstream	v1	7.4	-0.1
downstream	v2	7.4	1.5
downstream	v3	7.4	-1.7
upstream	v1	-5.5	-0.1
upstream	v2	-5.5	1.5
upstream	v3	-5.5	-1.7

Figure 10. *Six configurations of the jet and the micro-vane spacing.*

the configurations, it is seen that both downwash and upwash regions are augmented, which clearly indicates augmentation of the primary vortex generated by the vane. It should be noted, though, that the hybrid effect in configuration v3 differs from the other two, as two vortices generated off the vane and the jet only begin to interact, and a rather broad and weakened imprint of the resulting flow is captured.

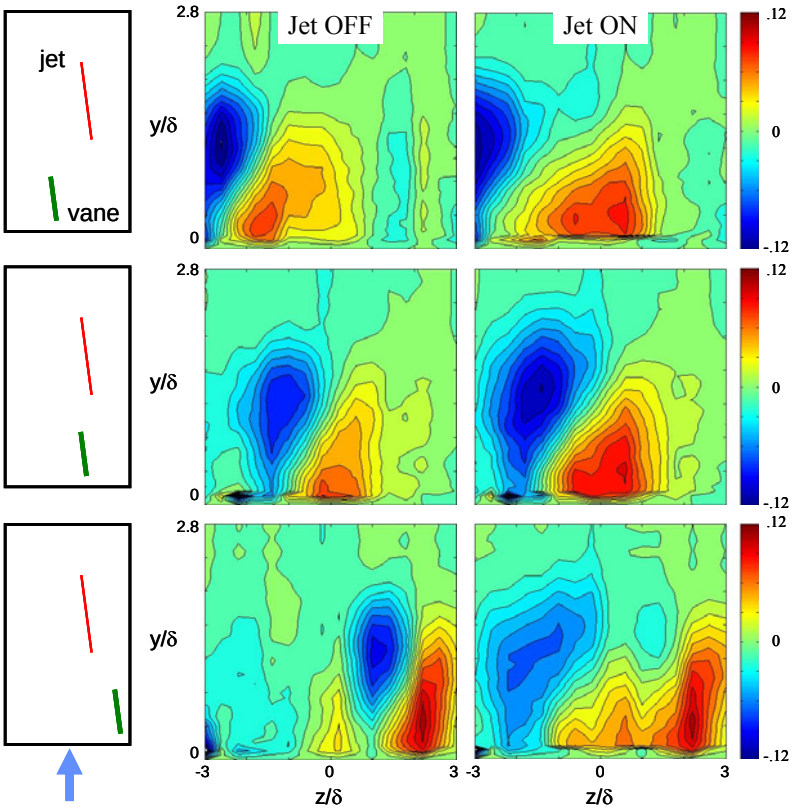

Figure 11. *Contours of the streamwise velocity difference DU/U0 for the passive (middle column) and hybrid (right column) control for the three configurations having the upstream vane (Figure 10): v2 (top row), v1 (middle row), and v3 (bottom row).*

To illustrate effect of the hybrid control on the boundary layer, a cross-stream integral measure is assessed from the relative spanwise changes in the shape factor h of the cross stream velocity distribution in the case of passive and hybrid control configuration v1 (Figure 12). Each $h(z)$ profile is shown as a relative change to the baseline shape factor (no control). The most prominent feature of $h(z)$ is that the induced streamwise vortices lower the shape factor through most of the affected spanwise domain in either case. These data also show that passive and hybrid control have very similar domains where the shape factor is increased, as that hybrid control only shifts it outboard. The main downwash region for the passive control is approximately bound by $-1 < z/\delta < 1.5$, where h is decreased. Hybrid control both extends the spanwise extend of the favorable effect and increases its magnitude, as localized decrease in h reaches about 10%.

Analogous to Figure 11, all three cases of the hybrid control having the vane downstream from the jet are shown in Figure 13. First, it is noteworthy that the effects of three studied configurations on the flow are very similar, regardless of whether the vane precedes the jet or vice versa. Two top configurations v2 and v1 induce a clear augmentation of the primary vortex off the vane, once the jet is activated in tandem regardless of which control element is in the leading position. The third configuration v3 in the present case shows even more prominently that individual vortices are initially

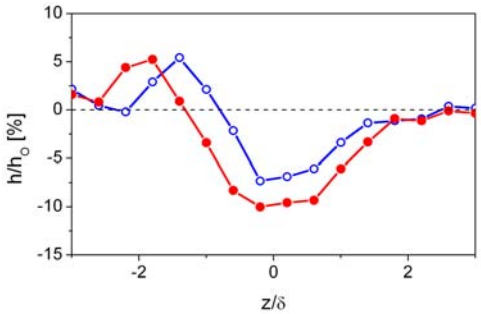

Figure 12. *Spanwise distribution of the relative boundary layer shape factor h for the passive (○) and hybrid (●) flow control for configuration v1 (Figures 10 and 11).*

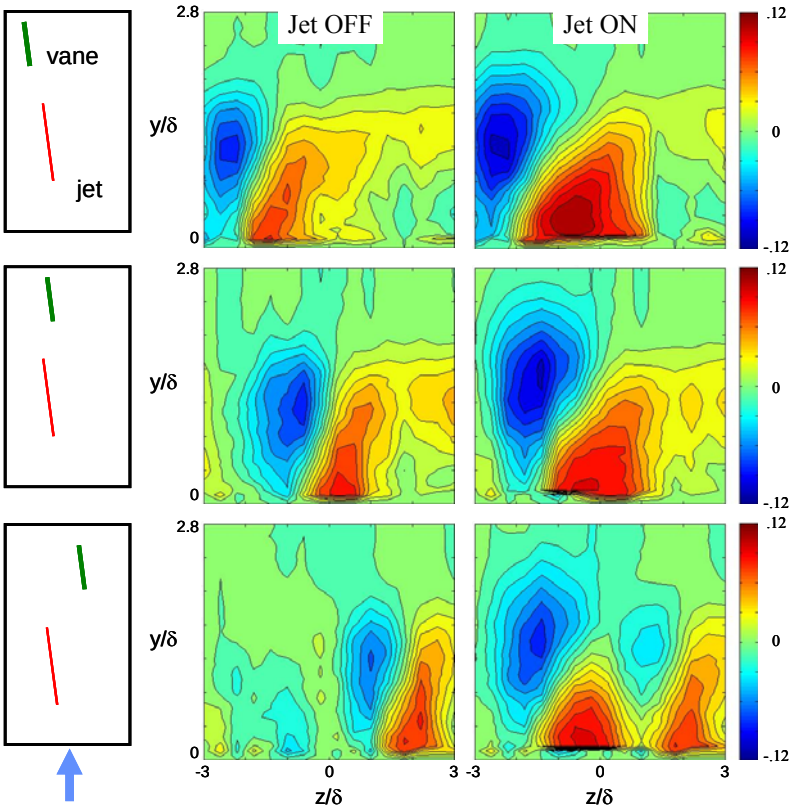

Figure 13. *Contours of the streamwise velocity difference $\Delta U/U_0$ for the passive (middle column) and hybrid (right column) control for the three configurations having the downstream vane (Figure 10): v2 (top row), v1 (middle row), and v3 (bottom row).*

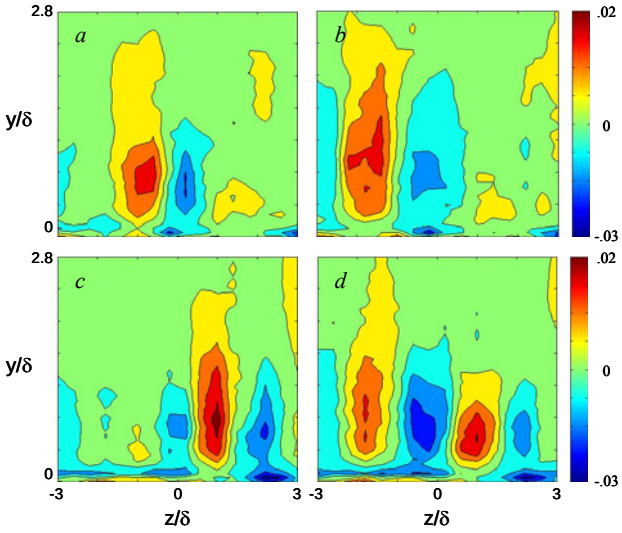

Figure 14. *Contours of the cross-stream velocity V/U0 for the passive (a, c) and hybrid (b, d) control for the v1 (a-b) and v3 (c-d) configurations shown in Figure 13.*

spaced far enough apart to prevent their coalescence at the measurement plane. Hence, the Jet ON case (Figure 13*c*) indicates two nearly separate vortices that are initially interacting.

In general, representation of downwash and upwash regions only in terms of the mean streamwise velocity component U, as it is conveniently done in this paper, is not sufficient to characterize a vortex. Therefore, two cases of successful and unsuccesfull vortex pairings from Figure 13, namely configurations v1 and v3, are further presented in terms of the mean cross-stream velocity component V, relative to the baseline flow (Figure 14). The passive control in either case results in a pair of adjacent upward and downward motions that indicate rotation associated with the streamwise vortex. In the case of configuration v1, activation of the hybrid control augments and enhances that primary vortex created off the vane. Contrary to this scenario, after the jet is activated in tandem with the vane in v3 configuration, there is an isolated jet-induced vortex and adjacent weakened primary vortex off of the vane that only begins to interact with the jet vortex. Clearly, conclusions drawn about the vortex dynamics from the V fields are identical to those from analysis of the ΔU fields in Figure 13 and, for redundancy, most results in this paper are presented only in terms of ΔU fields.

Analogous to assessment about the hybrid flow control influence of the boundary

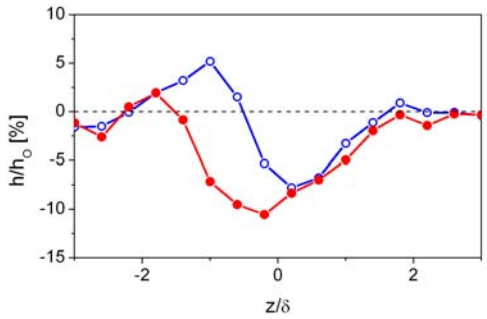

Figure 15. *Spanwise distribution of the relative boundary layer shape factor h for the passive (○) and hybrid (●) flow control for configuration v1 (Figures 10 and 13).*

layer in Figure 12, a cross-stream integral measure in terms of the shape factor h spanwise distribution is shown in Figure 15 for the case of passive and hybrid control configuration v1. The main downwash region for the passive control is approximately bound by $-0.5 < z/\delta < 1.8$, while the upwash induces an increase in the shape factor relative to the baseline flow at $-2 < z/\delta < -0.5$. As the hybrid control is activated, there is a twofold effect on the boundary layer relative to exclusively passive control: a favorable decrease in the BL shape factor is extended up to $z/\delta \approx -1.5$, while at the same time unfavorable effect in increasing h is vastly suppressed.

Traditional flow control strategies aimed at counteracting the secondary flow in ducts generally attempt to create two duct-scale counter-rotating vortices with sense opposite to that produced naturally by the secondary flow in the duct. In previous studies (e.g., Anabtawi et al. 1999), it has been shown that an array of streamwise vortices must be generated such that they merge into a large-scale vortex downstream of the duct, which imposes considerations of the vortex source's sizes and spacing. It is this prerequisite that often dictates the packing density and number of devices which in turn determines the overall drag penalty due to the implementation of the passive flow control. In a hybrid system it is thought that that the number of vanes could be reduced to diminish baseline drag and the active flow control component could merge these resulting vortices to provide favorable global flow field restructuring. This approach is first tested by spacing two passive vanes apart until two vortices generated by the vanes do not merge at the measurement plane. In addition, a single synthetic jet is placed upstream from the vanes in the configuration described in Figure 16. The resulting composite fields of ΔU and V are shown in Figure 16*a-b*, and 16*c-d*, respectively. As expected, two vortices created by two passive vanes are detected not fully interacting in Figure 16*a* and *c*. When the jet is activated the vane-generated vortices merge into one larger coherent structure as indicated by the large domain of influence of diminished velocity deficit (Figure 16*b*) and by the cross stream velocity component (Figure 16*d*) which indicate only one zone of upwash and one of downwash.

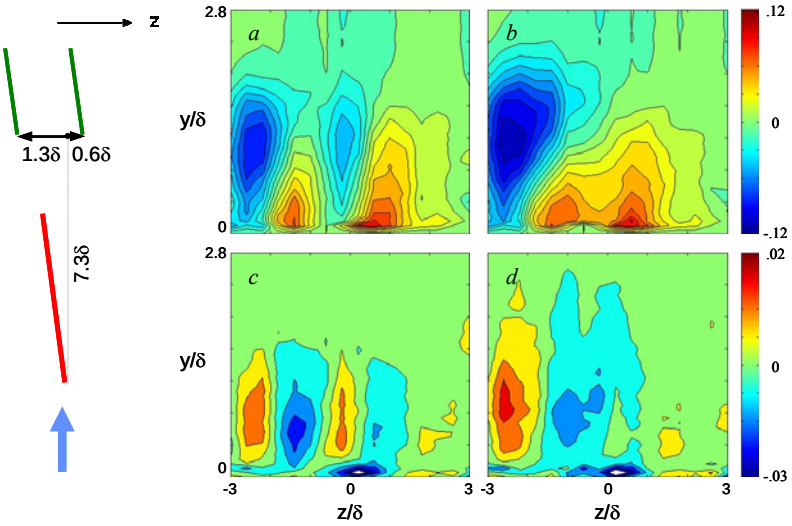

Figure 16. *Contours of the streamwise $\Delta U/U_0$ (a-b) and cross-stream V/U_0 (c-d) velocity difference for the passive (a, c) and hybrid (b, d) control by the jet in tandem with a micro-vane pair.*

Two shape-factor profiles $h(z)$ that correspond to Figure 16 are plotted in Figure 17 as integral effects of passive and hybrid control. The profile for

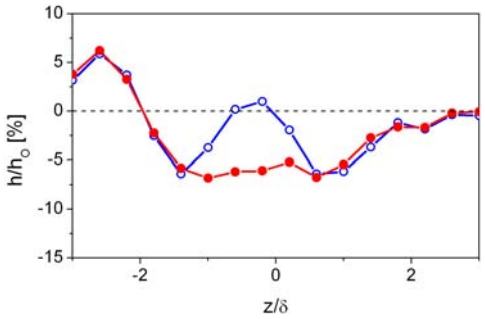

Figure 17. *Spanwise distribution of the relative boundary layer shape factor h for the passive (○) and hybrid (●) flow control for the case in Figure 16.*

the passive control exhibits two signatures of individual vortices, having the peak favorable effects at about $z/\delta \approx$ -1.4 and 0.8. It is notable that one vortex still induces the inherent increase in the shape factor due to associated upwash, but, owing to their commenced interaction, the upwash region associated with the other vortex is largely suppressed. The hybrid control connects two isolated favorable domains and flattens the favorable domain between $z/\delta \approx$ -1.4 and 0.8.

After learning how the active control element can enhance intentionally sub-optimized pair of vanes, further integration effort is undertaken in examining a configuration which more closely resembles a subset of actual array of vanes. For that purpose, three vanes are set in tandem with two interlaced jets. This study included variation of the vanes' spacing such that the generated passive-control effects included both near-optimal and sub-optimal vane configurations. Three tested configurations are outlined in Figure 18, where the vane spacing is varied among 1.6δ, 2δ, and 2.4δ. The resulting flow fields are shown in Figure 18 in terms of both ΔU and V raster plots. The first column in Figure 18 (Jet OFF) also has projections of the passive vanes labeled along the x-axis of the plots. For the closest vane spacing, sole passive control shows that the initial three vortices begin to interact upstream from the measurement plane, but do not merge into a single vortex by that point. Rather, two interacting vortical structures are detected at the measurement plane. Upon activation of the jets (Jets ON), it appears that each dominant vortical structure becomes enhanced. As the vanes are spaced further apart by 2δ (middle row), all three vortices generated by the vanes become visible

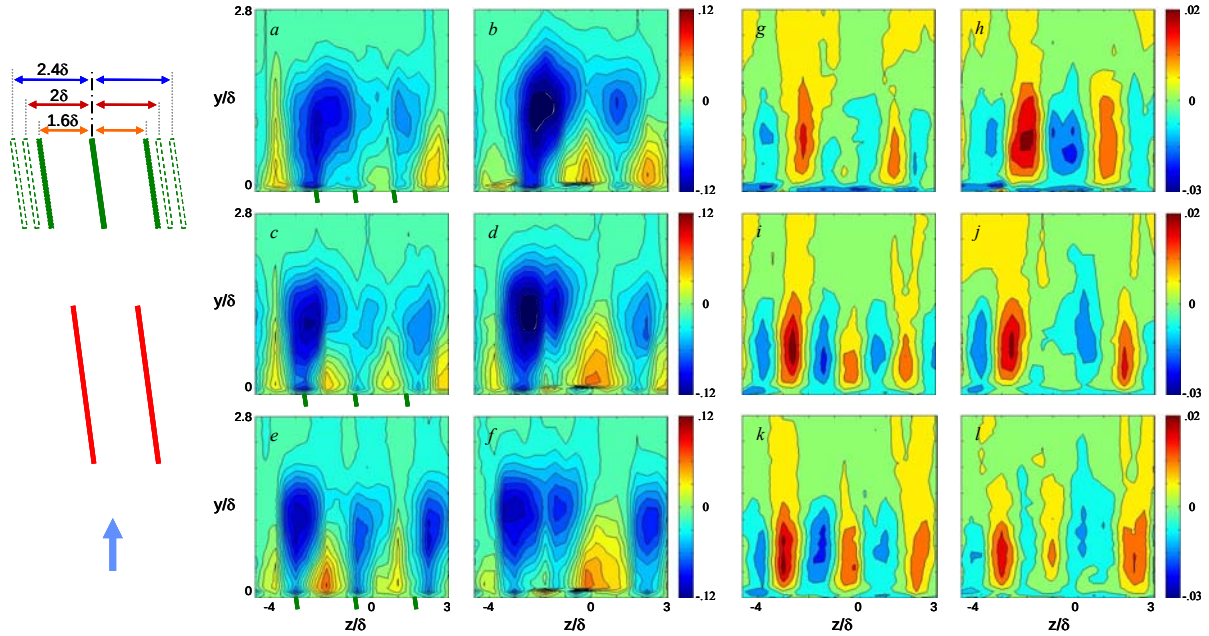

Figure 18. *Contours of the streamwise $\Delta U/U_0$ (a-f) and cross-stream V/U_0 (g-l) velocity difference for the passive (a, c, e, g, i, k) and hybrid (b, d, f, h, j, l) control by two jets in tandem with three micro-vanes spaced at 1.6δ (a, b, g, h), 2δ (c, d, i, j), and 2.4δ (e, f, k, l).*

at the measurement plane, as their interaction becomes spatially delayed. Activation of the jets not only enhances these passive-generated vortices, but also promotes their merging, as only signatures of two vortices are measured at the PIV plane. Finally, as expected, further increase in the vane spacing (bottom row) separates initial vortices formed off the vanes even more, and three distinct vortices are detected for the passive control case. Activation of the jets at this vane spacing is less effective in promoting merging of the vanes' vortices than in the previous configuration, although there is a strong enhancement of the streamwise vortices, but with a less coherent imprint due to their initiated interaction.

IV.3 Integrated Hybrid Configuration

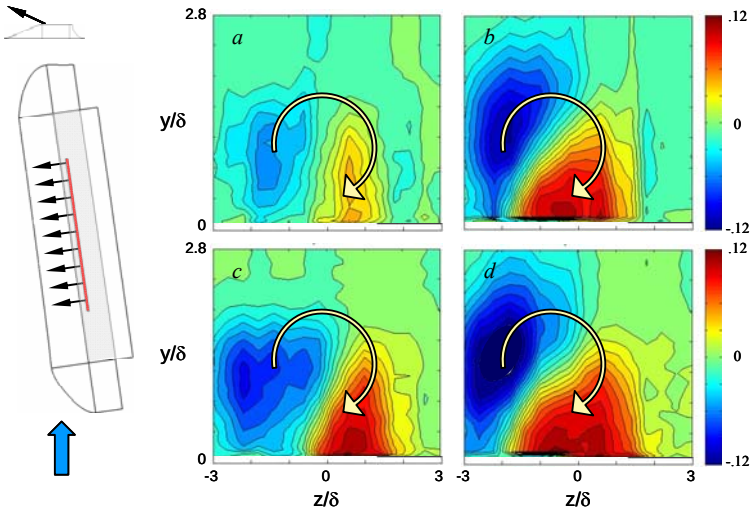

Figure 19. *Contours of the streamwise velocity difference $\Delta U/U_0$ for the passive (a, c) and hybrid (b, d) control for the integrated control device elevated 0.2δ (a-b) and 0.4δ (c-d) off the surface.*

Another approach to assembling active and passive control elements into a hybrid control device proposes direct integration of the active control into the passive element, i.e., the micro-vane in the present work. A major difference in this approach relative to any of the tandem approaches is that the hybrid control device would not generate any additional vortex entities, but would directly affect the primary vortex off the vane at its formation.

An initial exploration of such approach is done in this study by elevation of the synthetic jet actuator surface off the wall, thereby creating an unconventional passive 'vane'. The jet utilized in this study is internally identical to the one used in tandem configurations, as it is both yawed at 8° (as integrated into the vane), and skewed at 45°. Two elevations of such a 'vane' are considered 0.2δ and 0.4δ, selected to be somewhat below and above typical vane heights in the diffuser applications. These configurations are outlined in Figure 19, along with the composite fields of ΔU for the passive and hybrid control cases. First, as expected, strength of the streamwise vortex generated off the vane is directly proportional to the vane height, as the vortex generated by a taller vane generates much stronger velocity decrease and increase in velocity deficit near the wall. Nonetheless, in either case, activation of the

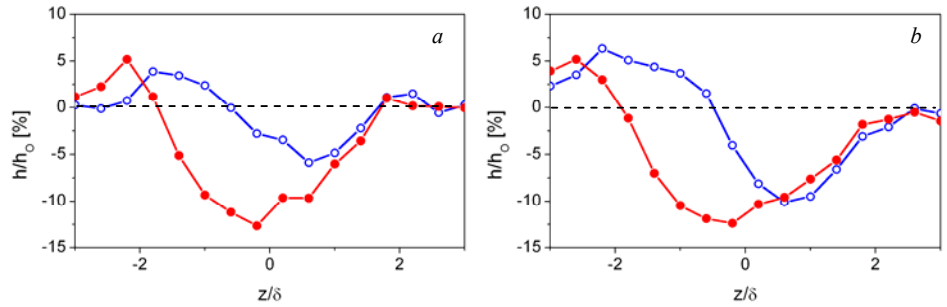

Figure 20. *Spanwise distribution of the relative boundary layer shape factor h for the passive (○) and hybrid (●) flow control for the integrated hybrid device in Figure 19 elevated 0.2δ (a) and 0.4δ (b) off the surface.*

integrated jet augments the primary vortex as the corresponding changes in velocity deficit increase both in magnitude and in affected domain.

The spanwise distributions of shape factor, $h(z)$, are plotted in Figure 20. Comparing the passive-control effect by a shorter (Figure 20*a*) and taller vane (Figure 20*b*), it is quantified that both favorable and unfavorable effects on the boundary layer are enhanced for the taller vane, both in their magnitudes and domains of influence. Hybrid control induces significant changes in the relative decrease in the shape factor and extension of such favorable spanwise domain for the shorter vane. As the passive effect is already rather pronounced in magnitude for the taller vane (Figure 20*b*), the main enhancement of the hybrid control is expressed by the nearly 2δ extension of the favorable domain across the span.

V. Conclusions

The present work focuses on an experimental investigation of the formation of streamwise vortices by exploiting the interaction between passive and active flow control elements within a duct flow. The evolution of these vortices is investigated at an upstream $M = 0.5$ on a converging-diverging wall in a small-scale wind tunnel that is designed to provide an adverse pressure gradient which mimics the pressure gradient within a typical offset diffuser. Single-sense vortices are formed and characterized using conventional passive micro-vanes combined with active synthetic jet actuators. This integration of passive and active control elements into a hybrid control device is motivated by the desire to reduce the flow losses that are associated with the presence of the micro-vanes, and to compensate for the reduced performance with "on-demand" fluidic actuation, while maintaining a minimum (fail-safe) level of effectiveness.

Two hybrid configurations that are characterized by the proximity of the jets to the vane were tested. In the first configuration, the jet actuators are placed in *tandem* with the vanes, and are oriented such that they are yawed to conform to the vane's yaw angle, and skewed so that the sense of the resulting streamwise vortices match the sense of the vane's vortices. It is shown that both the single vane and the jet engender individual streamwise vortices that induce measurable cross-stream spanwise downwash or upwash on opposite sides of their centerlines. However, the jet-induced vortex is unsteady, and temporally streamwise-segmented at the jet actuation frequency. Favorable augmentation of the vane-produced vortex is clearly demonstrated in several tandem configurations of a single jet with a single vane, regardless whether the jet is placed upstream or downstream of the vane. Additional configurations include subsets of arrays of vanes and jets which demonstrate augmentation and superposition of multiple active components onto a passive flow control array with varying degrees of optimization. In the second hybrid configuration, the jet is integrated into the vane which requires modification of traditional micro-vane geometry. Successful integration of the yawed/skewed synthetic jet which issues from the top of the vane is characterized by augmentation of the streamwise vortex that forms off the vane. It should be noted that this hybrid configuration does not generate any additional streamwise vortices relative to its counterpart passive configuration, but rather directly manipulates vorticity generated by the passive control components.

Acknowledgment

This work has been supported by NASA and the Boeing Company.

References

Amitay, M., Pitt, D., Glezer, A.,"Separation Control in Duct Flows," J. Aircraft., Vol. 39, No. 4, 2008, pp. 616-620.

Anabtawi, A.J., Blackwelder, R.F., Lissaman, B.S.P, Liebeck, R.H.,"An Experimental Investigation of Boundary Layer ingestion in a Diffusing S-Duct With and Without Passive Flow Control," AIAA Paper 99-0739, 1999.

Anderson, B.H., Gibb, J."Study on Vortex Generator Flow Control for the Management of Inlet Distortion," J. Prop. Pow. Vol. 9 No. 3 1993.

Anderson, B.H., Baust, D.H., Agrell, J. "Management of Total Pressure Recovery, Distortion and High Cycle Fatigue in Compact Air Vehicle Inlets," NASA/TM. 2002-212000, 2004a.

Anderson, B.H., Miller, D.N., Addington, G.A., Agrell, J. "Optimal Micro-Vane Flow Control for Compact Air Vehicle Inlets," NASA/TM. 2004-212936, 2004b.

Anderson, B.H., Miller, D.N., Addington, G.A., Agrell, J. "Optimal Micro-Jet Flow Control for Compact Air Vehicle Inlets," NASA/TM. 2004-212937.

Anderson, B., Tinapple, J., and Surber, L., "Optimal Control of Shock Wave Turbulent Boundary Layer Interactions Using Micro-Array Actuation," AIAA Paper 2006-3197, 2006.

Anderson, B.H., Mace, J.L., Mani, M.,"Active "Fail Safe" Micro-Array Flow Control For Advanced Embedded Propulsion Systems," AIAA Paper 09-741, 2009.

Bansod, P., Bradshaw, P.,"The Flow in s-shaped Ducts," *Aeronaut. Q.*, Vol. 23, 1972, pp. 131-140.

Berrier, B.L., Allan, B.G.,"Experimental and Computational Evaluation of Flush-Mounted, S-Duct Inlets," *AIAA Paper* 2004-764, 2004.

Berrier, B. L., Carter, M. B., and Allan, B. G., "High Reynolds Number Investigation of a Flush-Mounted, S-Duct Inlet with Large Amount of Boundary Layer Ingestion," NASA/TO-2005-213766.

Daggett, D.L., Kawai, R, Friedman, D." Blended Wing Body Systems Studies: Boundary Layer Ingestion Inlets With Active Flow Control," NASA/CR 2003-212670.

Gissen, A. N., Vukasinovic, B., and Glezer, A., Controlled Streamwise Vorticity in Diffuser Boundary Layer using Hybrid Synthetic Jet Actuation, AIAA Paper 2009-4021.

Jirásek, A., "Development and Application of Design Strategy for Design of Vortex Generator Flow Control in Inlets," AIAA Paper 06-1050, 2006.

Kawai, R.T., Friedman, D.M., Serrano, L.,"Blended Wing Body Boundary Layer Ingestion Inlet Configuration and System Studies", NASA/CR-2006-214534.

Lakebrink, M.T., Mani, M., Mace, J.L., Mcmillan, M.L."Numerical Investigation of Fluidic Hybrid Flow Control Influence on Boundary Layer Characteristics," AIAA Paper 09-2407, 2009.

Lin, J.C. "Review of research on low-profile vortex generators to control boundary-layer separation," Progress in Aerospace Sciences Vol. 38, 2002, pp. 389-420.

Owens, L.R., Allan, B.G., Gorton, S.A.,"Boundary-Layer-Ingesting Inlet Flow Control," J. Aircraft., Vol. 45, No. 4, 2008.

Peake, D.J., "Viscous Flow Control with Air-Jet Vortex Generators," AIAA Paper 99-3175, 1999.

Plas, A.P. Sargent, M.A., Madani, V. et. al. "Performance of a Boundary Layer Ingesting (BLI) Propulsion System," AIAA Paper 07-450, 2007.

Scribben, A.R., Ng, W., Burdiso, R., "Effectiveness of a Serpentine Inlet Duct Flow Control Technique at Design and Off-Design Simulated Flight Conditions ," J. Turbomachinery., Vol. 128, 2006, pp. 10-25.

Liebeck, R.H., "Design of the Blended Wing Body Subsonic Transport," J. Aircraft., Vol. 41, No. 1, 2004, pp. 332-339.

Smith, L.H., "Wake Ingestion Propulsion Benefit," Journal of Propulsion and Power, Vol. 9, No. 1, Jan.-Feb., 1993.

Tournier, S., Paduano, J.D."Flow Analysis and control in a Subsonic Inlet," AIAA Paper, 05-4734, 2005.

Vaccaro, J.C, Elimelech, Y., Amitay, M. "Experimental Investigation of Actuators for Flow Control in Short Inlet Ducts," AIAA Paper 10-862, 2010.